

Photomanipulation of the Mechanical Properties in a Liquid Crystal with Azo-Containing Bent-Core Mesogens

Marharyta Kurachkina,^[a] Hajnalka Nádas, ^[a] Mohamed Alaasar,^[b, c] Carsten Tschierske,^[b] and Alexey Eremin*^[a]

We demonstrate the reversible photomanipulation of the bulk mechanical properties in the azobenzene-containing bent-core liquid crystal. The azobenzene groups in the mesogens exhibit reversible cis-trans photoisomerization abilities. An unprecedentedly large reduction by the factor of more than 5 of the splay elastic constant in a cybotactic-type nematic phase was found under exposure to the UV. This opens up the possibility

to manipulate the mechanical properties of liquid crystals using light. The liquid crystal material is also distinguished by the sign inversion of low-frequency temperature-dependent dielectric anisotropy. Such behavior can be related to the presence of smectic-like nanoclusters both in the isotropic phase near the clearing point and in the cybotactic nematic phase.

1. Introduction

Stimuli-directed control of the mechanical and optical properties of matter is of paramount importance for the development of smart advanced materials. Azobenzene-based liquid crystals, exhibiting reversible photoisomerization upon irradiation with light, can be used for many applications in diverse fields, such as photonics, and photo-driven devices.^[1,2] Azo containing LCs are used as command surfaces for the alignment control^[3] and for controlling optical and structural properties of the mesophases.^[4–6] Optical writing is achieved by using cholesteric films containing light-driven chiral fluorescent molecular switches.^[7,8] Photomanipulation of the anchoring enables the photo-driven motion of the microparticles dispersed in an LC matrix.^[9,10] However, most of these applications are based on the light-manipulation of surface properties.^[1,11–15] In bulk, the photoisomerization leads to a shift in the phase transition temperatures. The effect of the photo-switching on the mechanical properties of liquid crystals is far less pronounced. To design such materials, it is necessary to explore new molecular designs containing extended structures with polar and chiral properties.

Liquid crystals formed by bent-core molecules (BCLCs) opened up a new field in soft matter with a wide variety of morphologies and structures that became an exciting new research area in the last decade of the twentieth-century.^[16–18]

Among the fascinating features of the BCLCs is the formation of chiral phases and nanostructures from achiral mesogens on a broad range of length-scales, observation of an exceptional flexoelectric response, and pronounced polar and smectic correlations in the nematic phases. The latter case marks the so-called nematic phases with cybotactic clusters. However, the nature of these clusters remains poorly understood.^[19–23] The model of the cybotactic N phase assumes the existence of smectic-like nanosized clusters exhibiting a layered supramolecular structure (typically skewed) with intrinsic biaxial orientational order within the nematic phase (designated N_{Cybc}). Although one can consider the smectic clusters as long-living fluctuations of the smectic order, their persistence over broad temperature range suggest that they are more complex than merely a pretransitional effect.^[20,24–26]


A combination of the ferroelectric LC order of bent-core mesogens and the photoswitchable nature of the azobenzene units has a great potential for the development of new multifunctional materials in which the polar response can be modulated with light. For this reason, azobenzene-based BCLCs attracted the attention of many researchers in recent years. 4-Cyanoresorcinol-based bent-core liquid crystals are distinguished for their formation of switchable orthogonal, weakly tilted, and heliconical phases.^[27–31]

In this paper, we demonstrate an exceptionally strong photoswitching of mechanical properties in azobenzene containing bent-core molecules incorporating 4-cyanoresorcinol as the central core unit. In addition, this compound exhibits cybotactic nematic and columnar phases. We explore the effect of the photoisomerisation on the optical and mechanical properties of the liquid crystal and demonstrate their reversible photoswitching. Nearly five-fold variation of the splay elastic constant and the sign inversion of the static dielectric permittivity have been observed in our study, which opens up new perspectives for applications of such material.

[a] Dr. M. Kurachkina, Dr. H. Nádas, Prof. A. Eremin
Otto von Guericke University, Inst. of Physics, 39016 Magdeburg, Germany
E-mail: alexey.eremin@ovgu.de

[b] Dr. M. Alaasar, Prof. C. Tschierske
Martin Luther University Halle-Wittenberg, Kurt Mothes Str. 2, D-06120
Halle (Saale), Germany

[c] Dr. M. Alaasar
Department of Chemistry, Faculty of Science, Cairo University, Giza, Egypt

 © 2020 The Authors. Published by Wiley-VCH Verlag GmbH & Co. KGaA. This is an open access article under the terms of the Creative Commons Attribution License, which permits use, distribution and reproduction in any medium, provided the original work is properly cited.

Materials and Methods

Materials

We investigated a bent-core mesogen with a 4-cyanoresorcinol core and with two rod-like azobenzene wings synthesised as reported in^[32,33] (Figure 1). The octyloxy homologue was chosen for its widest nematic range in the series. This compound exhibits a high-temperature nematic phase distinguished by the occurrence of the SmC-type cybotactic clusters (N_{CybC}). The mesophase extends over forty degrees which makes this compound a very convenient system for investigation. On cooling, the nematic phase transforms into a rectangular columnar phase Col_{rec} which persists down to crystallization.

Methods

Experimental studies were made in ITO glass cells with sandwich electrodes. We used Axiolmager D1 polarising microscope (Carl Zeiss GmbH) equipped with the programmable hot stage FS1 (Instec, USA) and the Berek compensator for birefringence measurements. For dielectric spectroscopy measurements, we used 10 μm thick ITO cells with a rubbed polyimide coating for the planar alignment and the resistance of 10 Ohm. The material was introduced into the cells using capillary suction in its isotropic state. The dielectric measurements were made using Solatron 1260 A impedance analyser (Ametek, USA) in the frequency range from 10 Hz to 10 MHz. To observe magnetic and electric Frederiksz transitions, we used electrical capacitance measurements of a liquid crystal cell by the impedance analyser at 5 kHz. Magnetic field varied from 0–700 mT. To extract the elastic constants, we fit the field-dependence of the dielectric permittivity using the standard procedure documented in literature.^[34]

Generation of the optical second harmonic (SHG) was measured using a confocal microscope TCS SP8-Leica. A tunable IR laser ($\lambda = 880 \text{ nm}$) was used as a fundamental light. As a liquid crystal device, we used 6 μm cells with interdigitated IPS electrodes. An electric field was applied by an arbitrary-wave generator (TTi) with a field

amplitude varying from 0 to 120 V at 10 Hz. Fundamental light was incident normally to the planarly LC cells. The SHG signal was collected by a photomultiplier tube at 440 nm. Photoswitching was studied under exposure to 360 nm UV lamp with variable power of up to 2.2 mW/cm^2 .

2. Results and Discussion

2.1. Optical properties

The nematic exhibits typical Schlieren textures on a bare glass substrate in the whole temperature range of the phase existence. In rubbed polyimide treated sandwich cells, a planarly aligned uniform texture occurs (Figure 2a).^[32] Earlier X-ray studies demonstrated a quite strong tilt in the clusters of the N_{CybC} phase reaching the value of 25 deg.^[32] On cooling the N_{CybC} is replaced by the rectangular columnar phase Col_{rec} distinguished by a typical spherulitic and mosaic textures (Figure 2b). The structure of the phase is given by a centred rectangular lattice with the lattice parameters $a = 3.7 \text{ nm}$ and $b = 4.6 \text{ nm}$.^[32] In previous studies, the low angle splitting of the XRD pattern in the N_{CybC} phase was attributed to the pretransitional smectic fluctuations occurring in compounds with a low-temperature smectic phase and not to the potential “biaxiality” of the nematic phase made of bent-core molecules.^[35] However, in our case, there is no smectic phase below the nematic.

One of the manifestations of the orientational order in nematics is birefringence. In the isotropic range, very small birefringence is observed close to the transition into the nematic state. This can be attributed to the surface ordering of the mesogens at the substrate. The birefringence Δn abruptly appears at the Iso- N_{CybC} transition reaching the value of 0.15

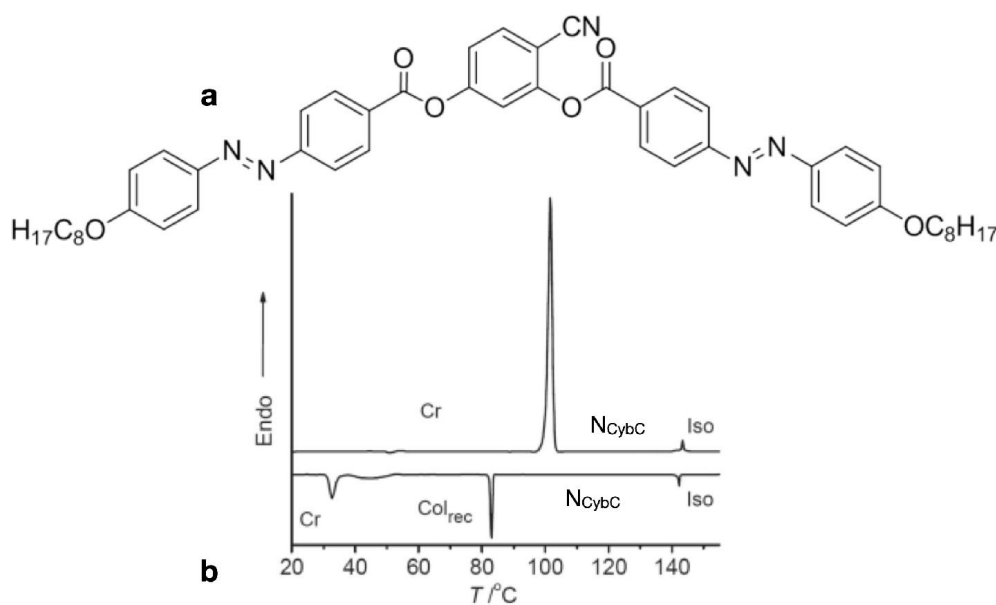


Figure 1. Chemical structure (a) and the DSC diagrams (b) of the bent-core liquid crystal. The phase transitions are: Cr 102 °C (Col_{rec} 83 °C) N_{CybC} 143 °C Iso, where Col_{rec} is a monotropic $B_{1\text{rev}}$ -type phase, only observed on cooling or second heating: Cr, Col_{rec} , N, and Iso represent crystal, columnar, nematic, and isotropic phases, respectively.^[32]

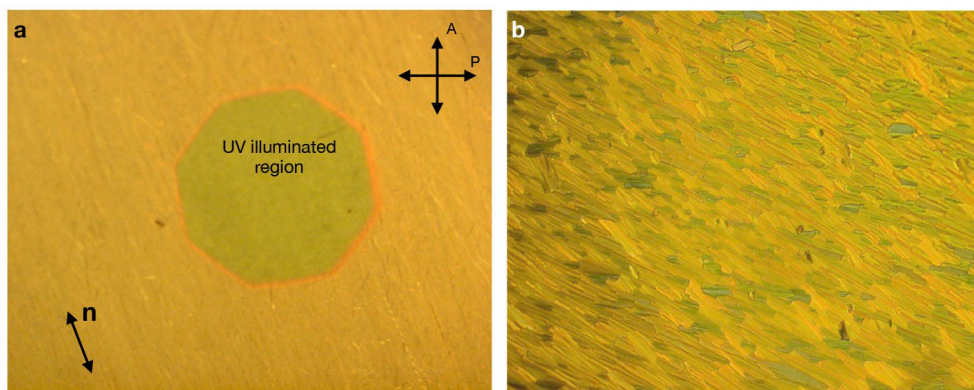


Figure 2. Polarized optical microscopy textures of the uniformly aligned nematic phase at $T = 130\text{ °C}$ (a) and the mosaic texture of the Col_{rec} phase at $T = 75\text{ °C}$ (b). The green spot in middle of (a) is produced by the local illumination with UV (365 nm, 2.4 mW) and results from the reduction of the Δn (5 micron rubbed polyimide cells).

just after the transition (Figure 3a). On decreasing temperature, birefringence continuously increases up to $\Delta n(T) \approx 0.33$ at the transition to the Col_{rec} phase. Such high birefringence values can be attributed to a high orientational order of the mesogens or their electronic structure. Haller approximation gives a simple relation between the orientational order parameter $S(T)$ and the temperature-dependent birefringence $\Delta n(t)$ in the nematic phase.

$$S = \left(1 - \frac{T}{T^*}\right)^\beta \quad (1)$$

where T^* and β are adjustable fitting parameters and T is the absolute temperature measured.

The fit of the birefringence data $\Delta n(t)$ using Haller formula is shown in Figure 3a. The equation fits well in the entire nematic range with fit parameters $\Delta n_0 = 0.38$ and $\beta = 0.18$.

Figure 3b shows the orientation order parameter obtained from the fit. $S(T)$ reaches its maximum value of 0.83. This value is high even for bent-core liquid crystals. One of the reasons responsible for such a high order parameter is the smectic ordering in the cybotactic nanoclusters. The orientational order in bent-core smectics is usually high due to the polar stacking

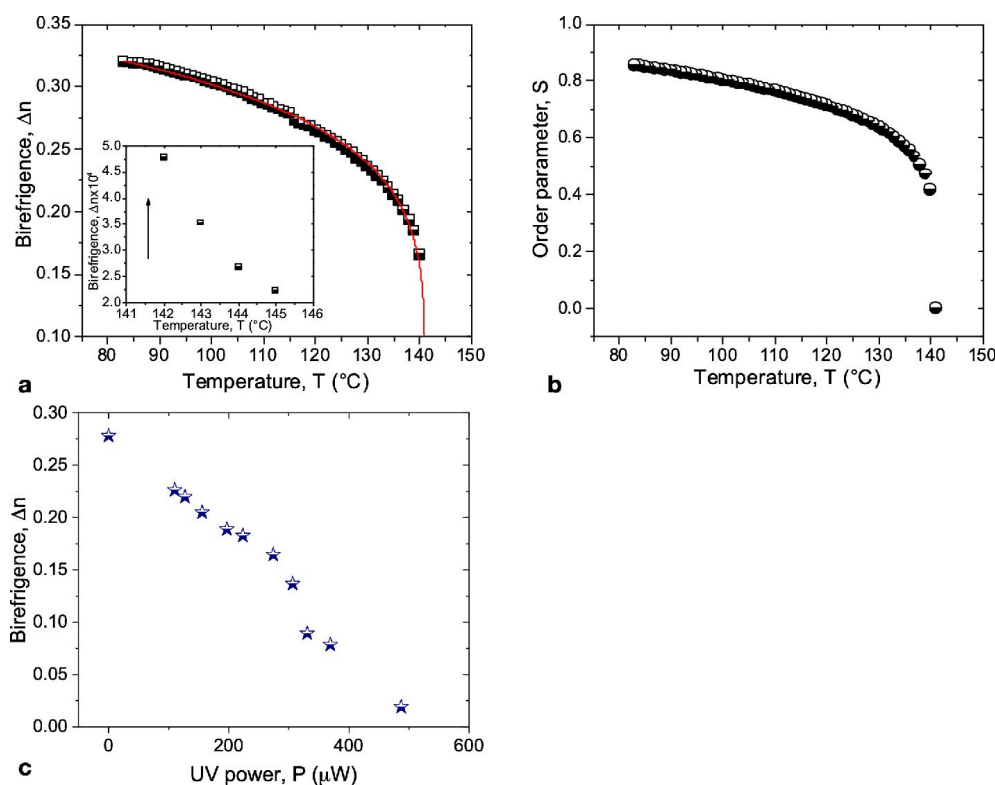


Figure 3. Temperature dependences of the birefringence (a) and the order parameter (b). (c) Reduction of birefringence under UV exposure.

of the mesogens. As the temperature decreases, the rotational motion of the molecules slows down resulting in a higher-ordered structure.

A distinctive feature of this material is its response to the UV. In polarized optical microscopy, a texture exposed to the UV changes its apparent color (Figure 2a). The birefringence continuously decreases with increasing UV power as shown in Figure 3c. This reduction to the athermal decrease of the orientational order parameter S through the steric distortion of the molecular packing by the photoisomers.

2.2. Polar dynamics

Polar dynamics manifest in the dielectric relaxation processes and the behaviour of the field-induced generation of optical second harmonic (SHG). Figures 4(a–c) show the dielectric spectra $\epsilon'(f)$ and $\epsilon''(f)$ recorded in planarly aligned cells in the nematic and columnar phases. The spectra reveal a single relaxation process in the frequency range from 100 Hz to 1 MHz in the nematic (Figure 4e). This process is related to the collective dynamics of the transversal dipole moment of the asymmetric mesogens in the nematic and columnar phases. The relaxation frequency exhibits Arrhenius behaviour with the activation energy $E_A = 0.24$ eV. This value is quite low due to

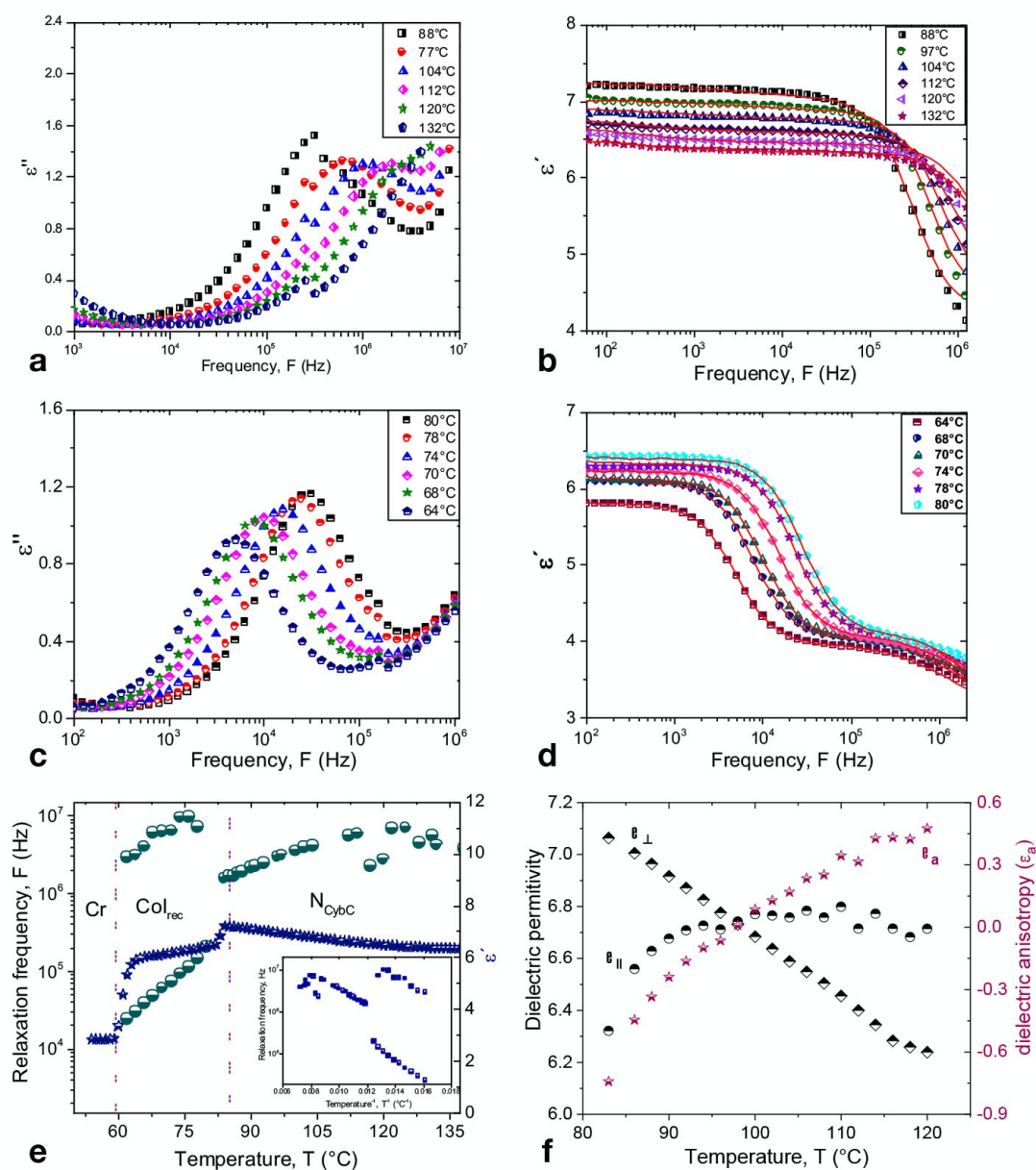


Figure 4. Dielectric spectra measured in the temperature range of the N_{CyBC} (a,b), and B_{1REV} phases (c, d). (e) Temperature dependence of the dielectric permittivity $\epsilon'(T)$ (measured at $f = 5$ kHz) and the relaxation frequency. Arrhenius plot of the relaxation frequencies is given in the inset. (f) $\epsilon_{||}$ and ϵ_{\perp} components of the dielectric permittivity and the temperature dependence of the dielectric anisotropy ϵ_a .

strong fluctuations of the long molecular axis in the nematic phase. At high temperature, in the isotropic phase, the relaxation is too fast to be accurately measured by the impedance analyser.

In the columnar phase, the rotational mode splits into two modes: a high-frequency (HF) and a low-frequency (LF) mode. Both modes exhibit Arrhenius-type behaviours with similar activation energies $E_A^{HF} = 0.44$ eV and $E_A^{LF} = 0.49$ eV. The antipolar ordering of the columns distinguishes the B1rev phase. The transversal dipoles exhibit two models corresponding to the scissoring motion of the polarisations of the columns. An increase in the activation energy compared to the nematic phase can be attributed to the stronger interactions of the molecules in a densely packed rectangular lattice. Orientational order in a liquid crystal phase results in the anisotropy of the dielectric permittivity. The components parallel to the nematic director ε_{\parallel} and perpendicular ε_{\perp} are determined from measurements on the liquid crystal at two orientations, respectively. Using a strong magnetic field, we align the nematic director parallel to the measuring field and determine ε_{\parallel} . Figure 4f shows the temperature dependences of $\varepsilon_{\parallel}(T)$, $\varepsilon_{\perp}(T)$, and $\varepsilon_{\sigma} = \varepsilon_{\parallel} - \varepsilon_{\perp}$. The parallel component is nearly temperature independent. Only close to the transition into the columnar phase, an anomalous decrease of ε_{\parallel} can be observed. At the same time, the perpendicular component exhibits a pronounced temperature dependence decreasing with increasing temperature. Due to the asymmetry of the mesogen, the transversal component of the permanent dipole moment cannot be averaged out by the rotations along the short molecular axis.

At the same time, the antipolar correlations grow for the longitudinal component. ε_{\parallel} decreases and the contribution from the parallel component of the permanent molecular dipole moment diminishes. This results in a strong temperature dependence of ε_{\perp} and even the sign inversion of the ε_{σ} . De Jeu et al. reported a similar effect in a rodlike mesogen with a strong permanent dipole in the vicinity of the N-SmA transition.^[36] In our case, the smectic correlations in the cybotactic N_{cybc} phase drive antipolar correlations of the polarisation.

Polar correlations in condensed phases also manifest in the generation of the optical second harmonic. Conventional calamitic rod-shaped liquid crystals with deformation-free nematic phases with quadrupolar order are not SHG active. Symmetry breaking at surfaces and the flexoelectric polarisation may result in an observable SHG. External electric fields are able to break the symmetry and result in polar order in the nematic. Mesogens have extended electron donor-acceptor system along each rod-like segment of the molecule, giving them a high hyperpolarisability. However, in the polar correlations are usually low, and the resulting polarisation usually is small. Collective polar behaviour, however, may result in a considerable polarisation and observable SHG.

Figure 5 shows the electric field strength dependence of SHG signal at different temperatures both in the nematic phase and the isotropic phases near the clearing point. No residual SHG was observed in the absence of an electric field. Only

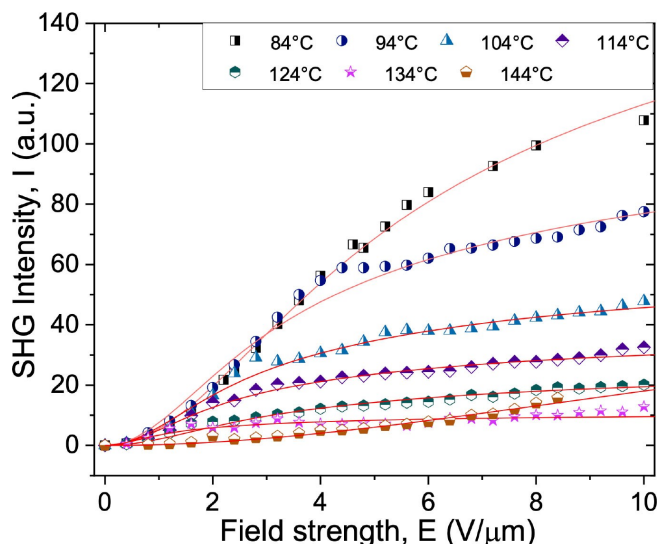


Figure 5. Electrically induced SHG signal $I_{2\omega}(E)$ measured in an IPS cell at a frequency $f = 10$ Hz.

upon application of an electric field, the SHG signal appeared and increased continuously with increasing field strength and without a seeming threshold. This behaviour is attributed to the collective response of the polar mesogens organised in nanoclusters. An increase in the SHG intensity at higher values of the electric field during cooling of a liquid crystal is associated with an increase in the number and size and distribution of smectic-like nanoclusters in the nematic bulk. As noted earlier, cybotactic clusters were found not only in the nematic phase but were also obtained in an isotropic phase in the vicinity of the clearing point.

2.3. Mechanical Properties

One of the consequences of the broken rotational symmetry in the nematic phase is the orientational elasticity of nematics. This is the key property, which is exploited in numerous applications of liquid crystals in technology. The elastic constants determine the speed of optical switching of LC displays. Experimentally, the splay and bend elastic constants are determined from the variation of the LC cell capacitance through the magnetic-field induced Fredericksz transition. The splay elastic modulus K_{11} is directly related to the threshold voltage $V_{th}^{k_{11}}$ by:

$$K_{11} = \varepsilon_0 \Delta \varepsilon \left(\frac{V_{th}^{k_{11}}}{\pi} \right)^2 \quad (2)$$

The bend elastic constant K_{33} influences the steepness of the variation of capacitance above the threshold and can be deduced using a fitting by:

$$\frac{V}{V_{th}^{K_{11}}} = 2\pi^{-1}(1 + \gamma \sin^2 \theta_m)^{\frac{1}{2}} \int_0^{\frac{\pi}{2}} \left(\frac{F_k}{F_{\xi} F_{\gamma}} \right)^{\frac{1}{2}} d\theta \quad (3)$$

where $F_k(\theta) = 1 + k \sin^2 \theta_m$, $F_{\xi}(\theta) = 1 - \sin^2 \theta_m$, $F_{\gamma}(\theta) = 1 + \gamma \sin^2 \theta_m$, $k = \left(\frac{K_{33}}{K_{11}} \right) - 1$, $\gamma = \left(\frac{\epsilon_{\parallel}}{\epsilon_{\perp}} \right) - 1$ and θ_m is the director angle in the midplane of the liquid crystal cell with planar alignment.^[37] Figure 6a shows the splay K_{11} and bend K_{33} elastic constants of the investigated compound as a function of the reduced temperature. K_{11} increases monotonically with decreasing temperature. It nearly doubles over the temperature range of the nematic phase, whereas, K_{33} remains almost temperature independent. There are two striking features in this behaviour: K_{11} is exceptionally high and $K_{33} \ll K_{11}$. The latter feature, the elastic anomaly, is frequently observed in the bent-core nematics and the nematic phases formed by dimers exhibiting the twist-bend-nematic phase^[16]. The azo-groups in the wing units of the mesogen are responsible for a remarkable response to the UV exposure. Exposing a planar cell to a UV illumination at $365 \text{ nm} \pm 20 \text{ nm}$, we observe a systematic reduction of the birefringence, which is attributed to the

reduction of the orientational order of the mesogens. The effect is fully reversible. A UV-induced state rapidly relaxes when the exposure is terminated. The relaxation occurs thermally as well as under the exposure to the long-wave light in the blue range of the visible spectrum. The strongest effect, however, manifests in the behaviour of the Frank elastic constants. Exposure of the sample to the UV results in a shift of the magnetic Frederiks transition to lower fields. This shift indicates a drastic reduction of the splay elastic constant K_{11} . Since we do not have an exact value of the diamagnetic anisotropy, we use both electric and magnetic Frederiks transitions to measure the Frank elastic constants. Low values of the dielectric anisotropy do not allow us to estimate the parallel component of the dielectric permittivity ϵ in an electric field. However, measurements of both components of ϵ can be obtained in a magnetic field. The result of the measurement of K_{11} in the range of positive ϵ_a is shown in Figure 6b. The photoisomerisation results in both a drastic reduction of K_{11} and a change of the character of the temperature dependence. The slope of $dK_{11}(T)/dT$ is significantly reduced and K_{11} is nearly temperature independent. Photoswitching of the elastic constant is completely reversible and K_{11} rapidly relaxes to its initial value when the UV exposure is terminated (Figure 6b). The effect of

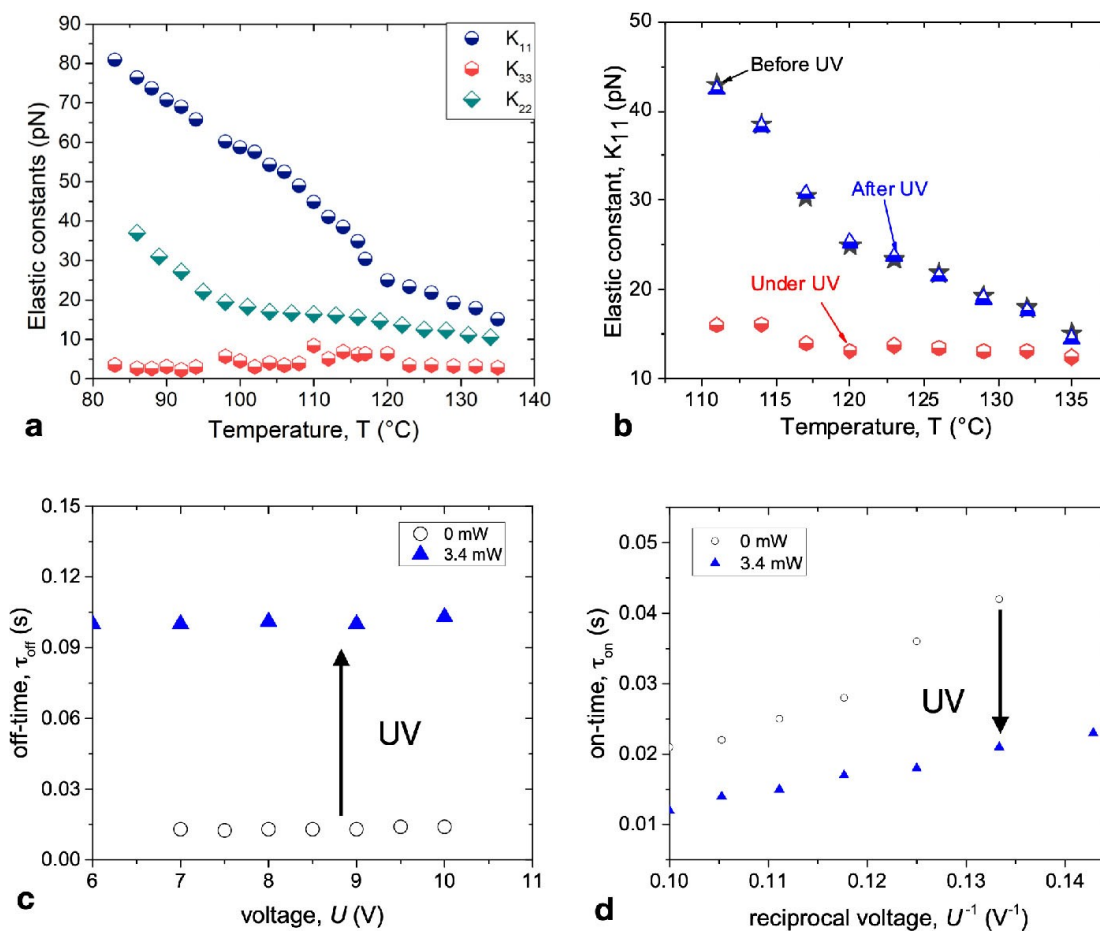


Figure 6. a) Temperature dependence of the splay (blue stars) and the bend (red circles) elastic constants. b) The effect of the UV illumination on the splay elastic constant: K_{11} before UV exposure (squares), under (circles) UV, and after (triangles) termination of the UV exposure. c and d) Switching times depending on applied voltages: a) on-time, b) off-time. The measurements are done in a $2 \mu\text{m}$ planarly aligned cell at $T = 120^\circ\text{C}$.

UV on the mechanical properties is manifested in the switching times of a nematic cell (Figure 6c,d). The rate of electrooptical switching is an essential parameter for designing LC devices for applications. The switching time is determined by the elastic constant and the viscosity of the liquid crystal.

Figure 6 c,d shows electro-optical switching times for a 2 micron cell with a planar alignment of the nematic director. The switching-on time τ_{on} exhibits a typical dependence proportional to the inverse driving voltage. Exposure to the UV results in a strong reduction of τ_{on} , which is especially well seen for high driving voltages. The off-time τ_{off} is independent on the driving voltage and it increases with increasing intensity of the UV illumination, since the elastic back-driving torque becomes reduced, but the viscous torque remains constant.

The photoisomerisation results in a drastic configurational change of the mesogens. The shape of the mesogens becomes strongly perturbed since both mesogenic wings can exhibit photoisomerisation. Using MOPAC software, we simulated molecular shapes for the *trans/cis*, *cis/cis* and *cis/trans* isomers (Figure 7). As shown in Figure 7b, the *cis/cis* isomer has a zig-zag shape. Under the assumption of fast rotation around the long molecular axis, the mesogen takes on an effective rod-shape. In the shown conformations both isomers have comparable values of the dipole moment 4.62 D for the *trans/trans* and 4.59 D for the *cis/cis* isomers. Assuming fast flipping of the mesogens around the short axis, the component of the dipole moment along the molecular bow is 3.0 D for *trans/trans* and 3.1 D for the *cis/cis* isomer. The alpha polarisability tensor α_{ij} (where $i, j = x, y, z$) was computed for both isomers in the molecular coordinate system. Assuming

fast rotation around the long molecular axis, the α_{ij} is averaged yielding the component $\alpha_{||}$ parallel and perpendicular α_{\perp} to the long molecular axis. For the *trans/trans* isomer, the $\alpha_{||} = 642.8$ a.u. ($(1.030 \times 10^{-36}) \text{ Cm}^2 \text{ V}^{-1}$) and $\alpha_{\perp} = 825.5$ a.u. ($(1.361 \times 10^{-36}) \text{ Cm}^2 \text{ V}^{-1}$). For the *cis/cis* isomer, the $\alpha_{||} = 393.0$ a.u. ($(6.480 \times 10^{-37}) \text{ Cm}^2 \text{ V}^{-1}$) and $\alpha_{\perp} = 614.6$ a.u. ($(1.103 \times 10^{-36}) \text{ Cm}^2 \text{ V}^{-1}$). The *trans/cis* isomers have a rather hockey-stick shape.

As seen from these estimations, the polarisability of the bent-core mesogens has a negative anisotropy, i.e. the molecules are easier polarisable along the bow direction. However, the macroscopic polarisability determining the dielectric response depends on the precise conformation, the order parameter and the dipolar correlation between the molecules. Strong dependence of the static dielectric constant on the temperature suggests that the contribution of the permanent dipoles dominate the response.

At a given UV intensity, a stationary state establishes between all four possible stereoisomers, which can assume different conformations from almost linear via hokey stick like to strongly bent. Due to a large shape difference between the isomer and the two *cis/trans* (hockey stick-shaped), the *cis/cis* (rod-shaped) isomers perturb the order of the *trans/trans* (bent-core) isomers. Assuming that the tendency to smectic ordering results chiefly from the dense packing of the *trans/trans* isomers with bent-core conformations, we expect that the exposure to the UV suppresses or at least strongly reduces the formation of the cybotactic clusters. The same applies to the dipolar correlations which become perturbed by the presence of the *cis* isomers.

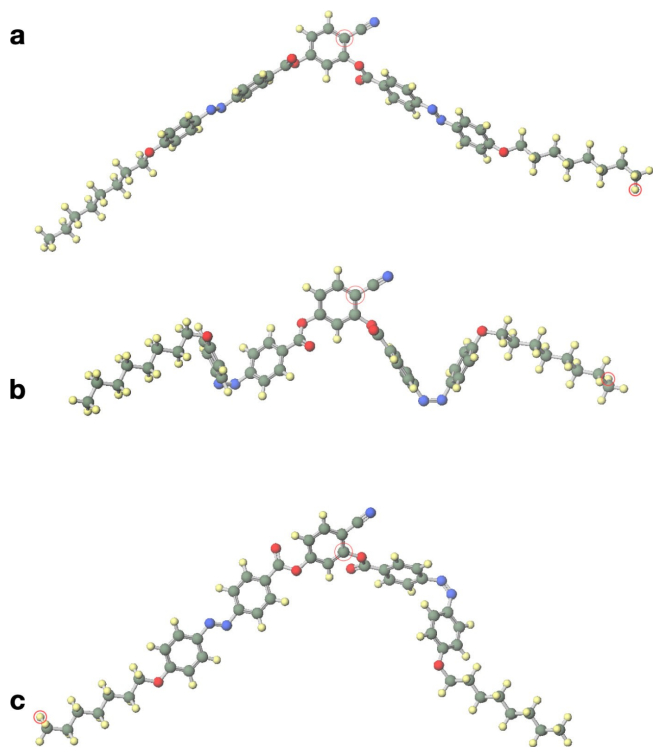


Figure 7. Model of the *trans/trans* isomer a) and *cis/cis* b) and the *trans/cis* isomers, simulated using MOPAC software.

3. Conclusions

In this study, we demonstrated photomanipulation of the optical and mechanical properties of the 4-cyanoesorcinol-based bent-core liquid crystal. This compound shows a strong temperature dependence of the static dielectric anisotropy exhibiting a sign inversion. Up to five-fold decrease of the splay elastic constant was observed under exposure to the UV. These unique properties of the liquid crystal are attributed to the enhanced smectic fluctuations, the presence of the cybotactic clusters, which structure is strongly affected by the photoisomerisation. Such materials have a significant potential for the design of multifunctional electro-optic and opto-mechanical materials.

Acknowledgments

This work was supported by the DFG (ER 467/8-2 and TS 39/ 24-2). Open access funding enabled and organized by Projekt DEAL.

Conflict of Interest

The authors declare no conflict of interest.

Keywords: azobenzenes · liquid crystals · mesophases · photoswitching

- [1] H. Yu, T. Ikeda, *Adv. Mater.* **2011**, *23*, 2149–2180.
- [2] O. S. Bushuyev, A. Tomberg, T. Frišćić, C. J. Barrett, *Journal Of The American Chemical Society*, **2013**, *135*, 12556–12559.
- [3] K. Ichimura, *Chem. Rev.* **2000**, *100*, 1847–1874.
- [4] H. K. Bisoyi, Q. Li, *Chem. Rev.* **2016**, *116*, 15089–15166.
- [5] R. S. Zola, H. K. Bisoyi, H. Wang, A. M. Urbas, T. J. Bunning, Q. Li, *Adv. Mater.* **2018**, *31*, 1806172.
- [6] M. Mathews, R. S. Zola, D.-K. Yang, Q. Li, *J. Mater. Chem.* **2011**, *21*, 2098–2103.
- [7] J. Li, H. K. Bisoyi, J. Tian, J. Guo, Q. Li, *Adv. Mater.* **2019**, *31*, 1807751–7.
- [8] H. K. Bisoyi, T. J. Bunning, Q. Li, *Adv. Mater.* **2018**, *30*, 1706512–35.
- [9] A. Eremin, P. Hirankittiwong, N. Chattham, H. Nadasi, R. Stannarius, J. Limtrakul, O. Haba, K. Yonetake, H. Takezoe, *Proc. Nat. Acad. Sci. USA* **2015**, 201419850.
- [10] P. Hirankittiwong, N. Chattham, J. Limtrakul, O. Haba, K. Yonetake, A. Eremin, R. Stannarius, H. Takezoe, *Opt. Express* **2014**, *22*, 20087.
- [11] H. Takezoe, O. Haba. Azodendrimers as a Functional Material. In C. M. Simionescu, editor, *Dendrimers*. IntechOpen, Rijeka, **2018**.
- [12] T. Seki, *Polym. J.* **2014**, *46*, 751–768.
- [13] T. Seki, S. Nagano, M. Hara, *Polymer* **2013**, *54*, 6053–6072.
- [14] K. Ichimura, Y. Suzuki, T. Seki, A. Hosoki, K. Aoki, *Langmuir* **1988**, *4*, 1214–1216.
- [15] H. Nádasi, R. Stannarius, A. Eremin, A. Ito, K. Ishikawa, O. Haba, K. Yonetake, H. Takezoe, F. Araoka, *Phys. Chem. Chem. Phys.* **2017**, *19*, 7597–7606.
- [16] H. Takezoe, A. Eremin. *Bent-Shaped Liquid Crystals: Structures and Physical Properties* Taylor & Francis Group, **20**, 7.
- [17] A. Jákli, O. D. Lavrentovich, J. V. Selinger, *Rev. Mod. Phys.* **2018**, *90*, 045004.
- [18] R. A. Reddy, C. Tschierske, *J. Mater. Chem.* **2006**, *16*, 907.
- [19] O. Francescangeli, M. Laus, G. Galli, *Phys. Rev. E* **1997**, *55*, 481–487.
- [20] O. Francescangeli, E. T. Samulski, *Soft Matter* **2010**, *6*, 2413.
- [21] C. Keith, A. Lehmann, U. Baumeister, M. Prehm, C. Tschierske, *Soft Matter* **2010**, *6*, 1704.
- [22] Y.-K. Kim, G. Cukrov, F. Vita, E. Scharrer, E. T. Samulski, O. Francescangeli, O. D. Lavrentovich, *Physical Review E* **2016**, *93*, 062701.
- [23] M. Alaasar, S. Poppe, C. Tschierske, *Liq. Cryst.* **2016**, *44*, 729–737.
- [24] N. Vaupotic, S. Curk, M. A. Osipov, M. Cepic, H. Takezoe, E. Gorecka, *Physical Review E* **2016**, *93*, 022704.
- [25] Y. P. Panarin, S. P. Sreenilayam, J. K. Vij, A. Lehmann, C. Tschierske, *Beilstein J. Nanotechnol.* **2018**, *9*, 1288–1296.
- [26] R. Balachandran, V. P. Panov, J. K. Vij, A. Lehmann, C. Tschierske, *Physical Review E* **2013**, *88*, 032503.
- [27] A. Eremin, S. Diele, G. Pelzl, H. Nadasi, W. Weissflog, J. Salfetnikova, H. Kresse, *Physical Review E* **2001**, *64*, 051707.
- [28] M. Alaasar, M. Prehm, M. G. Tamba, N. Sebastian, A. Eremin, C. Tschierske, *ChemPhysChem* **2015**, *17*, 278–287.
- [29] M. Alaasar, *Liq. Cryst.* **2016**, *43*, 2208–2243.
- [30] M. Alaasar, M. Prehm, S. Poppe, C. Tschierske, *Chem. Eur. J.* **2017**, *23*, 5541–5556.
- [31] S. P. Sreenilayam, Y. P. Panarin, J. K. Vij, V. P. Panov, A. Lehmann, M. Poppe, M. Prehm, C. Tschierske, *Nat. Commun.* **2016**, *7*, 11369.
- [32] M. Alaasar, M. Prehm, K. May, A. Eremin, C. Tschierske, *Adv. Funct. Mater.*, **2014**, *24*, 1703–1717.
- [33] M. Alaasar, M. Prehm, M. Nagaraj, J. K. Vij, C. Tschierske, *Adv. Mater.* **2013**, *25*, 2186–2191.
- [34] N. Sebastián, S. Belau, A. Eremin, M. Alaasar, M. Prehm, C. Tschierske, *Phys. Chem. Chem. Phys.* **2017**, *19*, 5895–5905.
- [35] N. Vaupotic, J. Szydłowska, M. Salamonczyk, A. Kovarova, J. Svoboda, M. Osipov, P. Ciecha, E. Gorecka, *Physical Review E* **2009**, *80*, 030701.
- [36] W. H. de Jeu, T. W. Lathouwers, P. Bordewijk, *Physical Review Letters* **1974**, *32*, 40–43.
- [37] D. Demus, J. Goodby, G. W. Gray, H. W. Spiess, V. Vill, *Physical Properties of Liquid Crystals*. Wiley-VCH Verlag GmbH, Weinheim, Germany, **1999**.

Manuscript received: June 2, 2020

Revised manuscript received: June 17, 2020

Accepted manuscript online: June 19, 2020

Version of record online: July 20, 2020